Fatigue behaviour of HIPed and stress relieved Ti6Al4V alloy specimens produced by SLM

J.S. Jesus[a*], L.P. Borrego[a,b], J.A.M. Ferreira[a], J.D. Costa[a], C. Capela[a,c]

[a] Univ Coimbra, CEMMPRE, Dept Mech Engn

[b] Department of Mechanical Engineering, Coimbra Polytechnic - ISEC, Rua Pedro Nunes, 3030-199 Coimbra, Portugal

[c] School of Technology and Management, Polytechnic Institute of Leiria, 2411-901 Leiria, Portugal

ABSTRACT

Fatigue behaviour of HIPed and stress relieved Ti6Al4V alloy specimens produced by SLM was analysed (R_ε = -1). The HIP process caused a microstructural transformation decreasing the hardness and monotonic properties that not allowed fatigue strength increase. A bilinear behaviour in the elastic strain-fatigue life curve was observed, because of Young´s modulus decrease during the cyclic elasto-plastic tests consequence of subgrains formation. The Smith-Watson-Topper and total strain energy density models showed a good concordance between predicted and experimental fatigue lives in notched samples.

Keywords: Ti6Al4V alloy, selective laser melting, strain-life fatigue curves, fatigue life prediction, cycle fatigue properties, S-N curves.

NOMENCLATURE

R_ε	Strain ratio
HIP	Hot Isostatic Pressing
SLM	Selective Laser Melting
LCF	Low Cycle Fatigue
R_a	Roughness Average
ε_a	Satrin amplitude
N_f	Number of cycles until failure
S-N	Curves: Stress vs Number of cycles until failure
σ-ε	Curves: Stress vs strain
wt.%	Weight percentage
H_2NO_3	Nitric acid
HF	Hydrofluoric acid
H_2O	Water
Δε	Strain range

k'	Cyclic strength coefficient
n'	Cyclic strain hardening exponent
σ_a	Stress amplitude
ε_a^*	Satrin amplitude of master curve
σ_a^*	Stress amplitude of master curve
$k^{¿}$	Cyclic strength coefficient of master curve
n'	Cyclic strain hardening exponent of master curve
ε_{a_p}	Plastic strain amplitude
ε_f'	Fatigue ductility coefficient
c	Fatigue ductility exponent
ε_{a_e}	Elastic strain amplitude
σ_f'	Fatigue strength coefficient
b	Fatigue strength exponent
E	Young´s modulus
kp	Material constant of energy density
αp	Material exponent of energy density
$\Delta W^{e+¿¿}$	Tensile elastic energy range at the material fatigue limit
ΔW_T	Total strain energy density range
σ_{max}	Maximum stress
k_t	Static concentration factor
σ_n	Nominal stress
k_f	Fatigue stress concentration factor

σ_{fu}	Fatigue strength for smooth specimens
σ_{fe}	Fatigue strength for notched specimens
q	Notch sensibility
σ_n	Nominal stress
$\Delta\sigma_{loc}$	Maximum local stress ranges
$\Delta\varepsilon_{loc}$	Maximum local strain ranges
FEM	Finite Element Method
SWT	Smith-Watson-Topper model
TEM	Transmission electron microscope
TKD	Transmission kikuchi diffraction
α	Microstructural phase of titanium
β	Microstructural phase of titanium alloys

1. INTRODUCTION

The Ti6Al4V alloy have been widely applied in both aerospace and biomedical industries due to its high strength, high thermal stability, and good corrosion resistance [1-3]. However, the machinability of titanium alloys manufactured by the traditional processing technologies presents some drawbacks, such as, sticking phenomenon, blade wear-out, material wastage and slow production times. The SLM process (Selective Laser Melting) presents great advantages such as, reduction of production steps, a high level of flexibility, a high material use efficiency, a near net shape production and also avoids the problems described previously.

The SLM process allows the production of complex parts with high precision through the successive powder layers deposition and laser melting, in a process understood as metal 3D print. The fatigue behaviour of parts produced by SLM is strongly affected by porosity defects, surface roughness and residual stresses, all resulting from the SLM process. The influence of surface roughness and internal defects, such as insufficient fusion and surface porosity, on fatigue performance of the Ti6Al4V alloy produced by SLM have been investigated by Wycisk et al.[4], Edwards et al. [5], Leuders et al.[6] and Cao et al.[7], showing a detrimental influence of these factors on the fatigue strength. Typically, the SLM parts are submitted to a post heat treatment in order to reduce/eliminate the residual stresses induced by to the high temperature gradients produced during the SLM process. Xuan and Nastac[8] obtained an increase in the fatigue strength of Ti6Al4V parts produced by SLM and submitted to a post-stress relief treatment, in comparison with the as-build parts.

Other authors, as Zhang et al.[9] and Atkinson and Davies[10], proposed the utilization of HIP (Hot Isostatic Pressing) treatment to reduce the porosity defects, surface roughness and introduction of favourable residual stresses, leading to an improvement of the fatigue performance. The HIP treatment is a process in which the material is subjected to both controlled temperature and isostatic gas pressure. The theory behind this process is to create a high enough hydrostatic pressure in the vessel so that any internal porosity (not surface connected) will collapse[11]. Chastand et al.[12] and Yu et al[13] applied the HIP treatment to Ti6Al4V specimens produced by SLM, using 920ºC of temperature and 120 MPa of pressure. The HIP process led to a porosity reduction that allowed a 10-15% increase in the fatigue resistance.

Wang et al.[14] and Carrion et al.[15] studied the fatigue behaviour of the Ti6Al4V alloy produced by conventional processes, by carrying out strain controlled fatigue tests. They obtained a cyclical softening when this alloy is subjected to strain amplitudes with a non-zero plastic component. Zhang et al.[16] compared the Low Cycle Fatigue (LCF) behavior of SLM Ti6Al4V and of wrought Ti6Al4V alloys, concluding that the wrought material showed a better fatigue performance for high strain levels due to the detrimental effect of the SLM defects, while, at low strain amplitudes, the SLM material presented a better fatigue performance. These authors also observed a cyclic softening behaviour of the materials produced by both processes.

Xu et al.[17] studied the LCF behaviour of the conventional processed Ti6Al4V alloy after being heat-treated at 925ºC and subsequently stabilized at 700ºC. They found that the fatigue life is highly influenced by the total strain amplitude, presenting a bilinear behaviour, i.e., a discontinuity with two regions with different slopes on the Coffin-Manson curve. For total strain amplitudes above 1-1.2%, the slope of the trendline is twice less than for total strain amplitudes below those values. This indicates that this alloy can have different cyclic deformation micromechanisms for different strain amplitudes. This bilinear behaviour has already been found in other metallic materials such as, nickel superalloys (Ye et al.[18] and Gopinath et al.[19]), aluminium alloys (Branco et al.[20] and Prasad et al.[21]) and titanium alloys (Gouthama and Singh,[22]).

In this work, fatigue tests were performed with Ti6Al4V alloy samples produced by SLM with circular cross-section for a strain ratio R_ε=-1. In addition, several complementary analyses were also performed, namely, metallography, hardness and tensile tests. Complementary analyses were performed in order to understand the variation in fatigue behaviour after the application of two different treatments: the stress relief treatment and the HIP treatment. Besides, fatigue life predictions were performed based on different prediction models for notched specimens and using the fatigue properties obtained in the experimental part of this study.

2. MATERIALS AND EXPERIMENTAL PROCEDURES

Fatigue test specimens were produced using Ti6Al4V alloy powder and the SLM process *3D Systems,* model ProX DMP 320. The energy density used to fabricate the specimens was 57 J/mm^3 and the thickness of each layer was 30 μm. The specimen's geometry was chosen following the recommendations of the ASTM E606 standard[23].

Fig. 1 shows the two specimen geometries used in this research, the loading direction and the build direction. Fig. 1a) presents the smooth specimens and Fig. 1b) shows the specimens with a semi-elliptical notch (a=0.8 mm and b=0.5 mm). All specimens were produced layer by layer in a reverse mesh at 45º using metal powder of Ti6Al4V (grade 23) Titanium alloy.

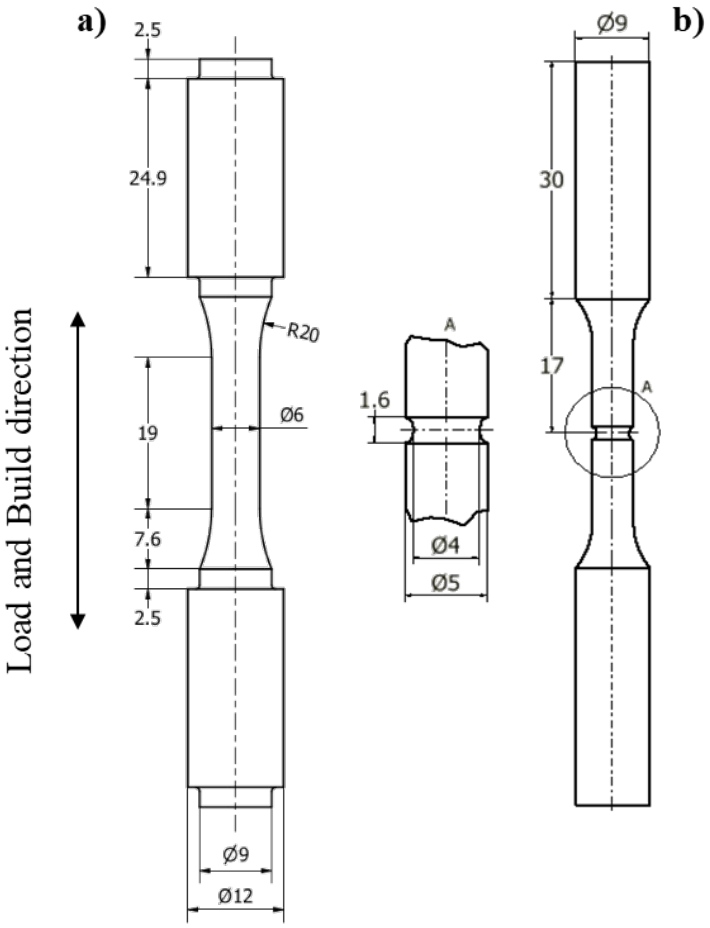

Figure 1. Specimens geometries (mm). a) specimens without notch, b) specimens with semi-elliptical notch.

For the smooth specimens, with the geometry illustrated in Fig. 1a), both HIP and residual stress relief treatments were applied, while for the notched specimens (Fig. 1b)) only the residual stress relief treatment was applied after the machining of the notch. The stress relief heat treatment consisted of slow and controlled heating up to 670°C, followed by a maintenance period at 670°C±15ºC for 5 hours and, finally, by cooling in air to room temperature. The HIP treatment was carried out submitting the specimens to a controlled heating up to 920 °C, followed by maintenance period at 920 ºC±15ºC for 2 hours in pressured chamber at 100 MPa. After the heat treatments, all specimens were

submitted to a polishing process in order to reduce the surface roughness (R_a=3.07 μm). After treatment by each of the two processes, samples were cut from the cross section of the specimens, and prepared following the recommendation of ASTM E3[24] to analyse the changes in microstructure and hardness. Afterwards, the surfaces were etched with Kroll's reagent (6% H_2NO_3 , 1% HF and 93% H_2O) as suggested in ASTM E407[25] and then observed and photographed in an optical microscope Leica DM 4000 M LED. As previously referred, the same samples were used to obtain the Vickers hardness following the ASTM E384-11e1[26], using a hardness tester Stuers Duramin 1 with 1 kg of test load and aleatory measurement indentation positions.

The monotonic tests were performed at room temperature in an Instron mechanical tensile/compression testing machine, model 4206, using a displacement rate of 2 mm/min and the specimen's geometry depicted in Fig. 1a). The tensile tests were performed according to the recommendations of ASTM B528-16[27] standard and using a 12.5 mm gauge length extensometer, Instron 2620-601, to acquire the elongation.

The fatigue tests were carried out in a Dartec servo hydraulic machine, applying a sinusoidal wave under fully-reversed strain-controlled conditions ($R_\varepsilon = -1$) and a constant strain rate ($d\varepsilon/dt$) of 8×10^{-3} s^{-1} as is recommended by ASTM E606[23] standard. The total strain amplitudes were in the range 0.3-1.875%. The strain was continuously controlled and acquired with the same extensometer used in the tensile tests, clamping it directly to the gauge zone of the specimen. Fatigue results were plotted mainly as ε_a-$2N_f$, S-N and σ-ε curves, presenting the strain amplitudes (elastic, plastic and total) against the number of reversions to failure, stress amplitude against the number of cycles to failure and stress amplitude against the strain amplitude, respectively. The half life criterion was used to analysis the cyclic stress-strain and strain-life responses of the materials in the two heat treatment conditions. The analysis of hysteresis loops at mid-life allowed to obtain the cyclical properties in the Ti6Al4V specimens built by SLM. Also, fatigue life predictions based in local approaches were performed for stress relieved notched specimens using the fatigue properties obtained in the tests.

3. RESULTS AND DISCUSSION

3.1. Metallographic analysis

Fig. 2 shows the microstructures obtained for each treatment. Fig. 2a) presents the microstructure of stress relieved specimens while Fig. 2b) shows the microstructure

obtained for the HIPed specimens. Both images show darker zones corresponding to primary columnar β phase grains and lighter areas corresponding to fine needles of the martensitic phase α (or α´). Greitemeier et al.[28] observed a similar morphology for the same material and manufacturing process, confirming a balance between the β and α phases in the stress relieved specimens (Fig. 2a)). On the other hand, when comparing Fig. 2a) and 2b) it is possible to see more dark zones (β phase) and less fine needles of the martensitic phase α (lighter areas), in the case of the HIP treatment (Fig. 2b)). The greater amount of the β phase in the specimens treated by HIP is due to the higher heating temperature in the HIP treatment (920ºC) that exceeds the transition temperature where the transformation of α phase to β phase occurs (882 ºC for pure titanium). Molaei et al.[29] also observed the same difference of microstructures after the applications of the two heat treatments. It was not possible to identify a denser structure in the HIPed specimens when comparing Fig. 2a) and 2b).

3.2. Hardness analysis

The HIPed samples showed an average hardness value of 350 HV1 while the stress relieved samples an average value of 405 HV1. The β phase is characterized by a lower hardness than the α phase. Therefore, the higher transformation of α phase to β phase during the HIP treatment leads to a loss of hardness of aproximadely 14 %.

3.3. Monotonic tests

The loss of hardness described above also leads to a loss of mechanical resistance in the specimens submitted to the HIP treatment and to an increase in ductility of about 33.5%, as shown in Table 1.

Table 1. Summary of the mechanical monotonic properties.

SAMPLE	σ_{UTS} **[MPa]**	σ_{ys} **[MPa]**	ε_f **[%]**	ε **[GPa]**
Sstres Relieved	1143	1107	19.7	126
HIPep	995	950	26.3	126
HIP vs Stress Relieved	-15%	-16.5%	+33.5%	-

The lower resistance and higher ductility obtained in HIP treated specimens can be explained by the higher transformation of α phase to β phase that occurs during this heat

treatment, given that the β phase is characterized by having lower hardness and greater ductility than the α phase.

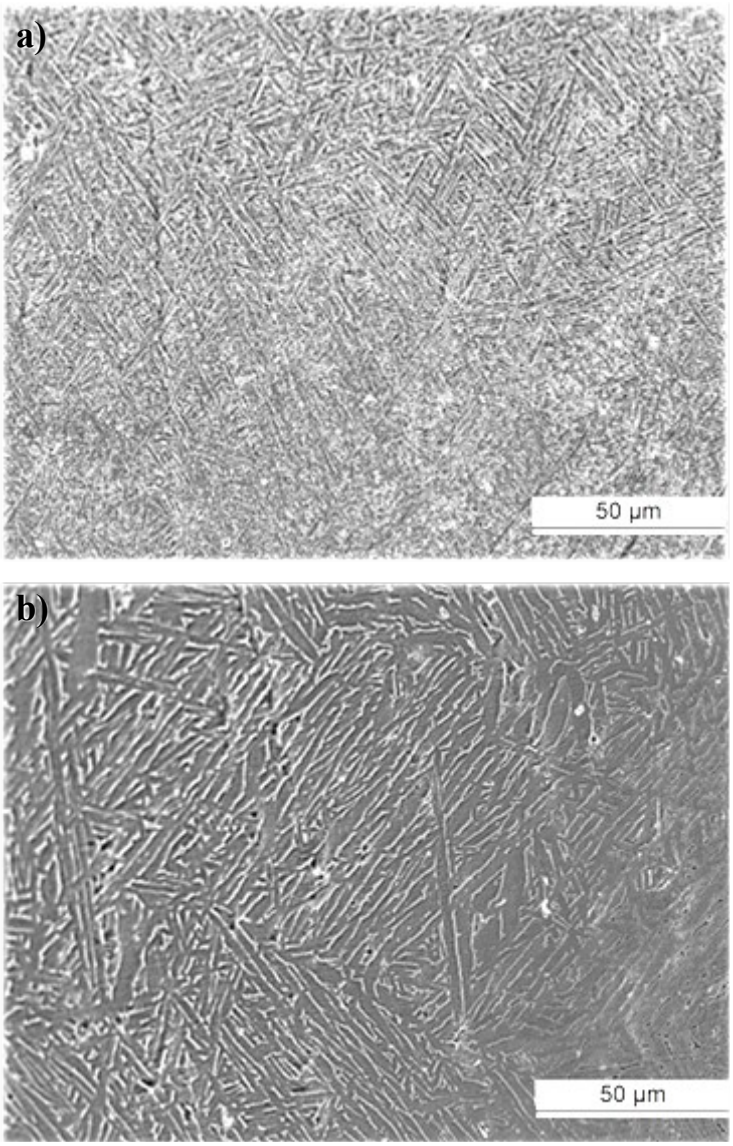

Figure 2. Optical metallographics of the specimens. a) stress relieved and b) HIPed.

3.4. Fatigue tests results

In this section the results of the fatigue tests will be presented in order to understand the effect of both heat treatments on the cyclic properties of the Ti6Al4V specimens built by SLM.

3.4.1. Hysteresis loops

Fig. 3a) and 3b) show exemplary hysteresis loops obtained in low cycle fatigue tests with a total strain amplitude of ε_a= 1.75% for the stress relieved and HIPed treatments, respectively.

In both treatments, the stabilization of hysteresis loops occurred after 17% of the total life, with a more pronounced cyclic softening in the case of the specimens subjected to the stress relief treatment, that is, the stress amplitude shows a greater reduction since the first cycle in comparison to stabilized cycles.

Fig. 3 shows that the Bauschinger effect occurred for both treatments, although it is more pronounced in the HIPed specimens. In fact, there is an asymmetry in the hysteresis loops with the maximum tensile stress being lower than the maximum compressive stress. This asymmetry is greater in the case of the HIPed specimens.

The analysis of the hysteresis loops also allows to conclude that the HIPed specimens showed greater ductility and greater deformation energy corresponding to the greater area within the hysteresis loops. These results agree with the transformation of the microstructure that occurs during the HIP treatment and its consequences in terms of the predominance of phase β with the properties already mentioned.

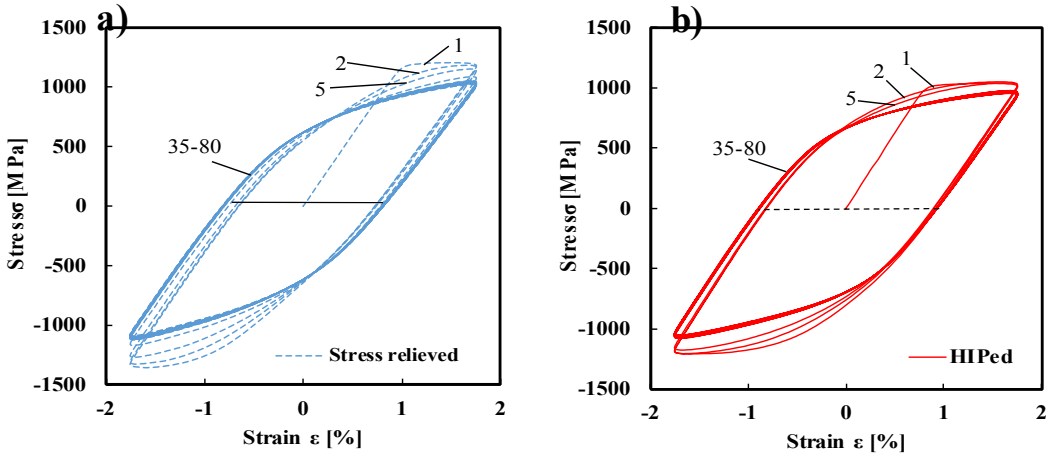

Figure 3. Hysteresis loops in elasto-plastic regime at ε_a= 1.75% for both heat treatments: a) Stress relief; b) HIP

3.4.2. Stress variation with fatigue life

Fig. 4a) and 4b) illustrate the variation of the stress ratio, $\sigma_{max}/-\sigma_{min}$, with the normalised fatigue life at various total strain ranges for stress relieved and HIPed specimens, respectively. For values of total strain ranges below 1.5% (predominantly elastic regime), the Bauschinger effect did not occur because the values of tensile stress and compression stress remained equal throughout fatigue life (hysteresis loops symmetry), whereby the stress ratio remained equal to 1. Fig. 4a) and 4b) also show that the

Bauschinger effect occurred in both series (stress ratio below 1), being more pronounced in the early fatigue cycles. This phenomenon was greater in HIPed specimens, where a higher difference is observed between the peak tension stresses and the peak compression stresses (Fig. 4b)).

For total strain ranges above 1.5% (elasto-plastic regime), it was found that the peak tensile and compression stresses undergo a gradual reduction in the first cycles of the fatigue tests in both heat treatments. Therefore, there is an initial cyclic softening followed by a maintenance period with practically constant stress values up to 90% of the total life. In the remaining 10% of the fatigue cycles there is a gradual drop in the stress peaks until rupture. Cyclic softening is more pronounced for specimens subjected to the stress relief treatment. For values of total strain ranges below 1.5% (predominantly elastic regime), there is no cyclic softening for both treatead series, since the peak stresses remain practically constant during the fatigue tests.

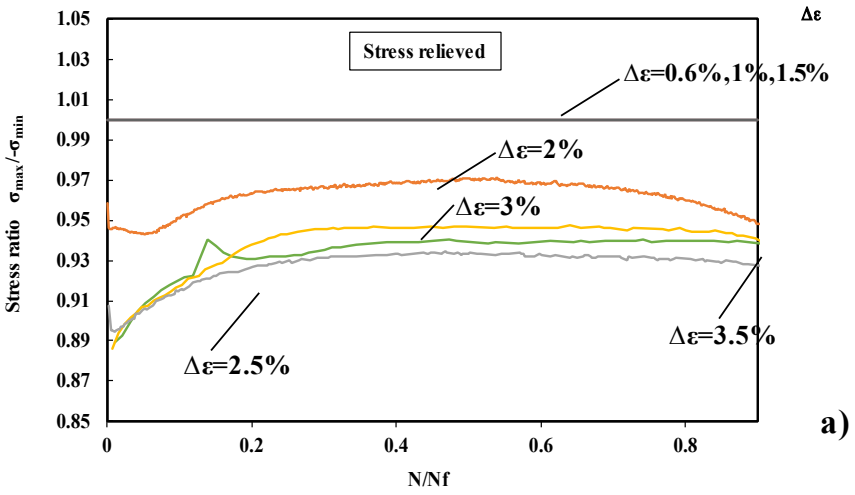

a)

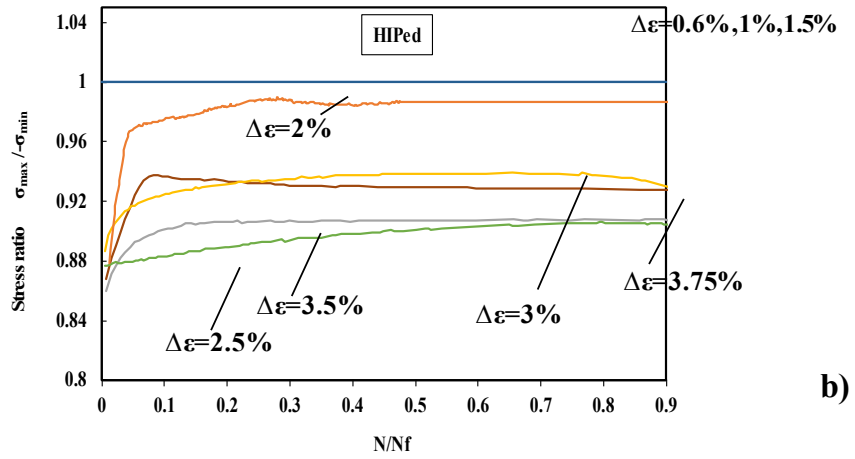

b)

Figure 4. Variation of stress ratio with the normalised fatigue life at various total strain ranges. a) Stress relieved specimens b) HIPed specimens.

3.4.3. Cyclic stress-strain behaviour

The cyclic stress vs strain curve can be written in the form (Ramberg-Osgood cyclic stress strain relation[30]):

$$\varepsilon_a = \frac{\sigma_a}{E} + \left(\frac{\sigma_a}{k'}\right)^{\frac{1}{n'}} \quad (1)$$

where k' and n' are, respectively, the cyclic strength coefficient and the cyclic strain hardening exponent, as summarized in Table 2. Fig. 5 shows the cyclic curves for both heat treatments.

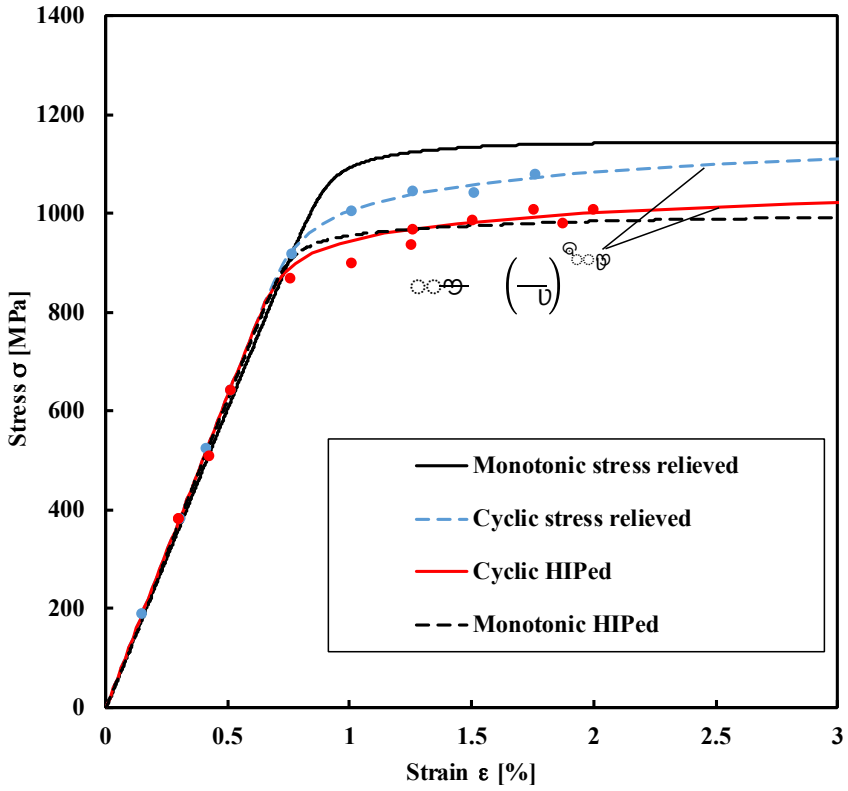

Figure 5. Cyclic stress vs strains curves.

In Fig. 5 it can be observed that the specimens submitted to the stress relieved treatment undergo a cyclic softening once the experimental points of the cyclic curve are below the monotonic curve, while, the HIPed specimens present a approximately stable behaviour once most of the cyclic stress-strain curve points are almost coincident with the monotonic curve. The hardened state of the stress relieved specimens leads to a

cyclic softening when subjected to cyclic straining. On the other hand, the HIPed specimens that are in an initial state of lower hardness, when subjected to cyclic straining did not undergo cyclic hardening or softening.

Table 2. Cyclic stress-strain curve properties.

k' [MPa]	**n'**	Stress relieved
1314	0.043	
k' [MPa]	**n'**	HIPed
1176	0.036	
k*[MPa]	n*	Stress relieved
2275	0.155	
k* [MPa]	**n***	HIPed
1695	0.111	

3.4.4. Masing material behavior

In Fig. 6 are plotted the cyclic Ramberg-Osgood equation and the mid-life hysteresis loops at different total strain ranges for both treatments. In both cases the cyclic curve and the upper branches at different strain amplitudes do not follow a unique curve, the material does not exhibit Masing-type behaviour, being therefore a non-Masing material. The non-Masing effect is associated with the alteration in the linear region of the stable circuits[31].

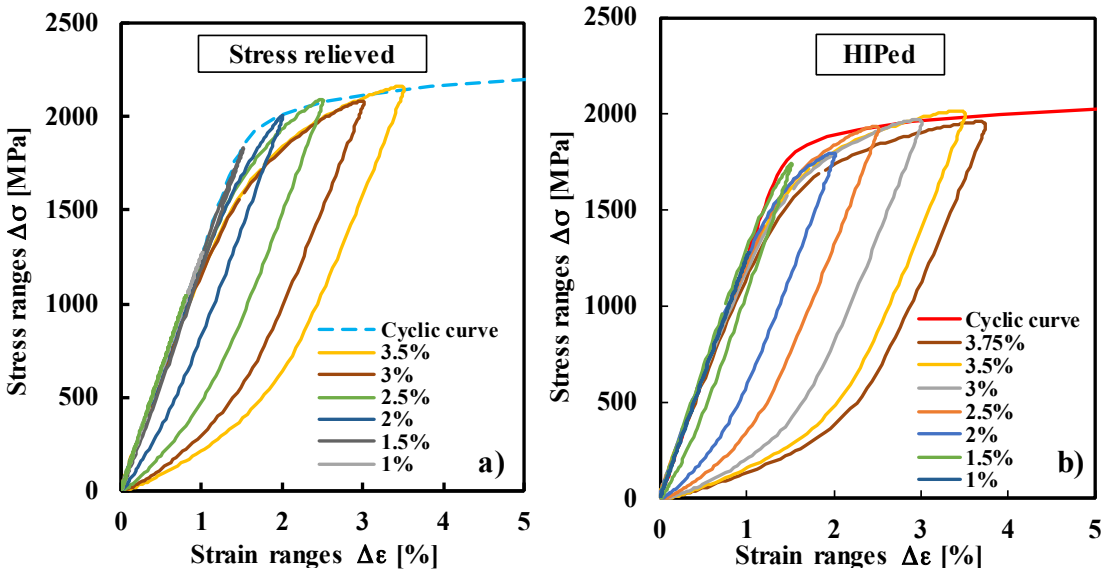

Figure 6. Cyclic Ramberg-Osgood model and mid-life hysteresis loops at different total strain ranges.

The deviation from non-Masing behavior can be examined by the construction of a master curve. The master curves were obtained by matching the loading branch of the stable hysteresis loops with the corresponding minimum strain range.

The equation of the master curve with respect to the new coordinate axes (ε_a^{*} and σ_a^{*}), corresponding to the minimum strain range can be expressed as Eq. 2.

$$\varepsilon_a^{*} = \frac{\sigma_a^{*}}{E} + \left(\frac{\sigma_a^{*}}{k^{*}}\right)^{\frac{1}{n^{*}}} \tag{2}$$

where asterisk (*) in superscript indicates that the corresponding parameters are measured with the new coordinate axes. Table 2 summarizes the parameters k^{*} and n^{*} for each specimen.

3.4.5. Strain-life curves

The elastic component of the total strain amplitude, ε_{a_e}, can be related with the number of reversals to failure, N_f, through the Basquin formulation[32] given by Eq. 3, where $\sigma_f^{'}$ is the fatigue strength coefficient, b is the fatigue strength exponent and E is the Young´s modulus.

$$\varepsilon_{a_e} = \frac{\sigma_f^{'}}{E}\left(2N_f\right)^{b} \tag{3}$$

Fig. 7 shows the variation of the number of reversals to failure with the elastic component of the total strain amplitude (in log-log scale) for a) stress relieved specimens and b) HIPed specimens. For both treatments a bilinear behaviour was observed (two linear regions with different slopes) in the elastic strain component depending of the total strain amplitude. This phenomenon is due to the dissimilar behaviour of the elastic strain component in the predominantly elastic regime (ε_a < 0.75% for stress relieved samples and ε_a < 0.68% for HIPed samples) and in the elasto-plastic regime (ε_a > 0.75% for stress relieved specimens and ε_a > 0.68% for HIPed specimens). The bilinearity in the elastic component of the total strain amplitude can be attributed to the variation of the Young's modulus during the fatigue tests in the elastic-plastic regime.This material exhibited a progressive reduction of the Young´s modulus when subjected to a total strain amplitude in the elasto-plastic regime (ε_a=1.5%), while,

in the predominantly elastic regime (ε_a=0.5%), the Young´s modulus remained constant along the fatigue life at the average value of 127502 ±362 MPa.

Yang et al[33] found that for some ductile materials the elastic modulus decreases according to the increase of plastic strain is due to the movable dislocation accompanying the pile-up of dislocations near to the grain boundary. This behaviour was also observed by Jyoti et al[34] in low cycle fatigue tests in an annealed titanium alloy Ti6Al4V obtained by conventional processes. These authors observed the formation of slip band, hexagonal network and sub-grain boundary using a transmission electron microscope (TEM) and transmission Kikuchi diffraction (TKD). At lower strain amplitudes evidences of the formation of slip bands and dislocation rearrangement was observed, while, in the case of higher strain amplitude, the development of defects in the structure and annihilation/rearrangement of dislocations occurs simultaneously.

As previously mentioned, the phase β is more easily deformed, as it is less hard and more ductile than the α phase. Consequently, the deformation in phase β causes progressive interactions of dislocations (dislocation pile-ups) with the α phase. This leads to the appearance of slip bands that gradually become new grain boundaries, leading to progressive divisions of β phase grains, giving rise to the formation of β phase sub-grains. This modification of microstructure contributes to the progressive increase in back stress and the decrease of the friction stress. As this variation increases with the accumulation of plastic deformation, a gradual decreasing of Young´s modulus occurred with the fatigue life. Moreover, this effect in the reduction of Young´s modulus will increase with the total strain amplitude. The progressive reduction of Young's modulus with the plastic strain amplitude causes a very significant reduction in the value of the fatigue strength exponent, b, of the Basquin relationship (lowest slope, see Table 3), in the elasto-plastic regime when compared to the predominantly elastic regime.

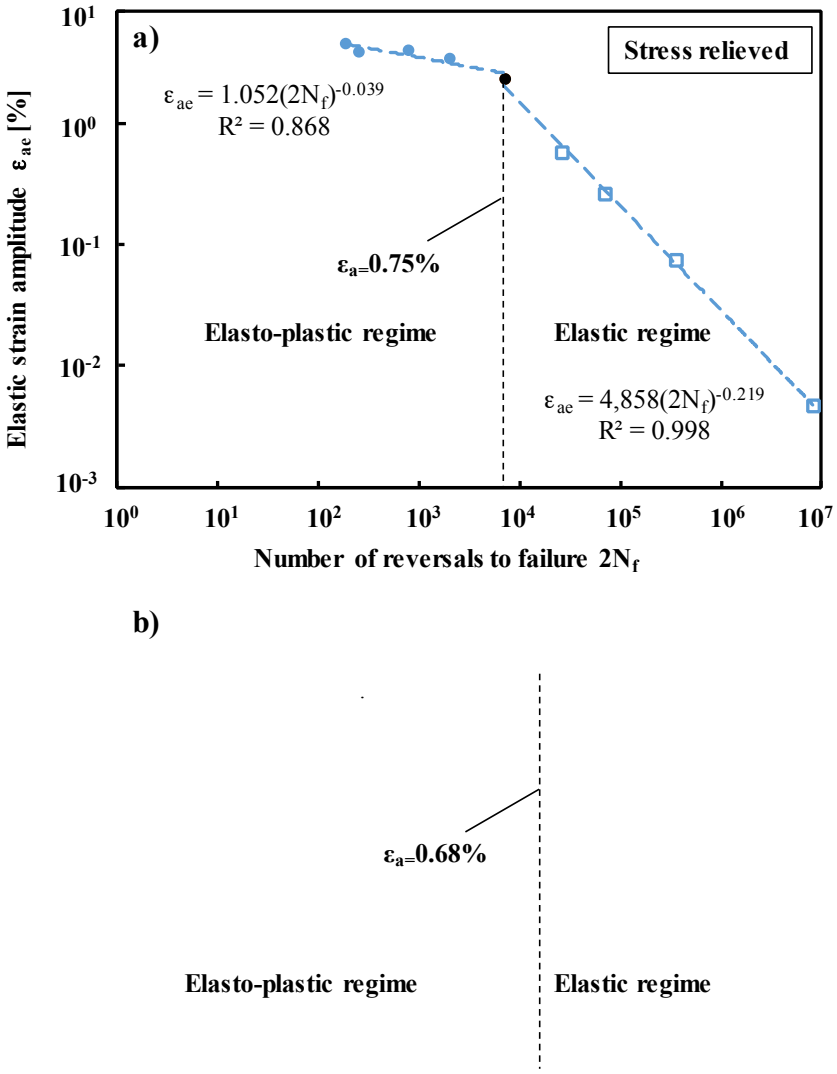

Figure 7. Baquin relationship. a) Stress relieved samples and b) HIPed samples.

The Coffin-Manson relationship[35-36], Eq. 4, relates the plastic component of the total strain amplitude, ε_{a_p}, with the number of reversals to failure, where $\varepsilon_f^{'}$is the fatigue ductility coefficient, and c is the fatigue ductility exponent.

$$\varepsilon_{a_p} = \varepsilon_f^{'}(2N_f)^c \quad (4)$$

Fig. 8 presents the Coffin-Manson relationship for both treatments. As can be observed, a linear relationship was achieved on a log-log scale, for both stress relieved and HIPed samples, fitting Eq. 4 with a high correlation coefficient in both cases.

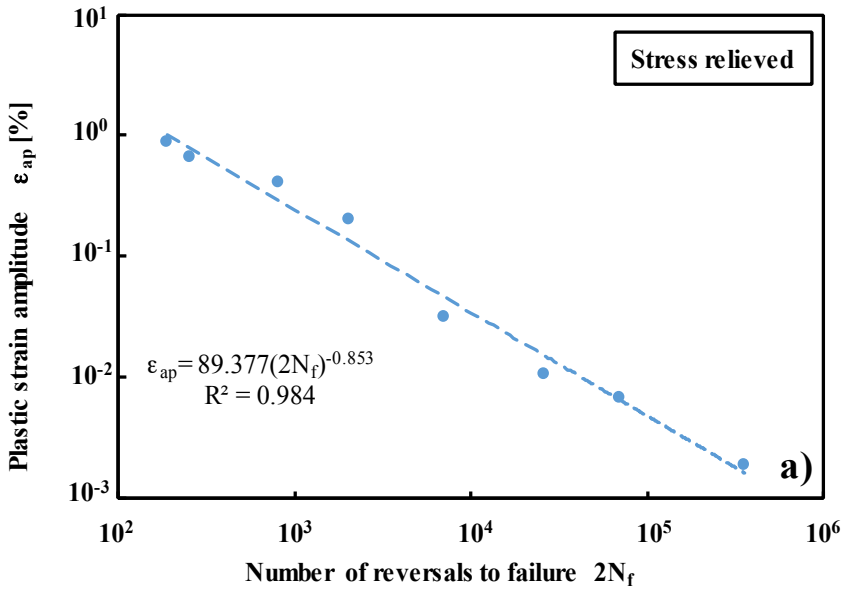

b)

Figure 8. Coffin-Manson relationship. a) Stress relieved samples and b) HIPed samples.

Morrow[37] proposed that the relationship between the metal's fatigue life and the total strain amplitude can be obtained by superimposing the elastic and plastic strain components. Therefore, adding Eq. 3 and 4, Eq. 5 is obtained.

$$\varepsilon_a = \varepsilon_f'(2N_f)^c + \frac{\sigma_f'}{E}(2N_f)^b \quad (5)$$

The variation of elastic, plastic, and total strain amplitudes with the number of reversals to failure is shown in Fig. 9a) and 9b) for the stress relief treatment and the HIP treatment, respectively.

a)

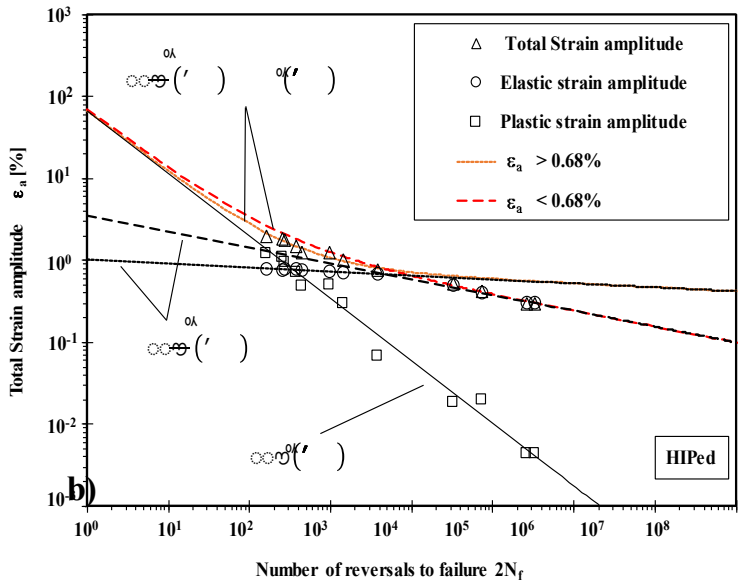

Figueres 9. Total, plastic and elastic strain amplitudes versus number of reversals failure. a) Stress relieved samples and b) HIPed samples.

In each of Fig. 9a) and 9b), two different curves were plotted to fit Eq. 5 in order to take into account the bilinear behaviour of this material. Table 3 summarizes the compilation of fatigue strength and fatigue ductility parameters for both heat treatments in the predominantly elastic tests (ε_a < 0.75% for the stress relieved sample and ε_a < 0.68% for the HIPed sample) and tests in elasto-plastic regime (ε_a > 0.75% for the stress relieved sample and ε_a > 0.68% for the HIPed sample).

Table 3. Fatigue strength, fatigue ductility and energy-based parameters for stress relieved and HIPed samples.

Stress relieved				
b	**c**	**σ'_f [MPa]**	**ε'_f [%]**	**$\varepsilon_a > 0.75$ [%]**
-0.050	-0.853	1328	89.4	
b	**c**	**σ'_f [MPa]**	**ε'_f [%]**	**$\varepsilon_a < 0.75$ [%]**
-0.219	-0.853	6129	89.4	
HIPed				
b	**c**	**σ'_f [MPa]**	**ε'_f [%]**	**$\varepsilon_a > 0.68$ [%]**
-0.039	-0.764	1311	67.2	
b	**c**	**σ'_f [MPa]**	**ε'_f [%]**	**$\varepsilon_a < 0.68$ [%]**
-0.193	-0.764	4416	67.2	

Stress relieved		
kp [MJ/m^3]	**αp**	**ΔW^{e+} [MJ/m^3]**
1524	-0.695	0.345
HIPed		
kp [MJ/m^3]	**αp**	**ΔW^{e+} [MJ/m^3]**
599	-0.573	0.215

In order to compare the difference in fatigue performance between the two treatments Fig. 10a) and 10b) show the strain-life and stress-life curves, respectively. Fig. 10a) shows that in the case of the ε-N curves, the difference in fatigue strength is minimal between the two treatments. In contrast, the S-N curves (Fig. 10b)) show higher fatigue strength for specimens with stress relieved treatment than for the HIPed specimens in the elasto-plastic regime. Despite the potential of the HIP treatment to decrease typically defects of SLM parts (porosity, lack of fusion, among others), the induced transformation of the microstructure and the consequent loss of hardness and mechanical resistance, leads to a decrease in fatigue resistance for LCF. On the other hand, in the high cycle fatigue regime (predominandly elastic tests), the fatigue performance for the two treatments was quite similar. The S-N curves also exhibited a

bilinear behaviour (two dissimilar slopes in the two regimes) by the reasons already explained.

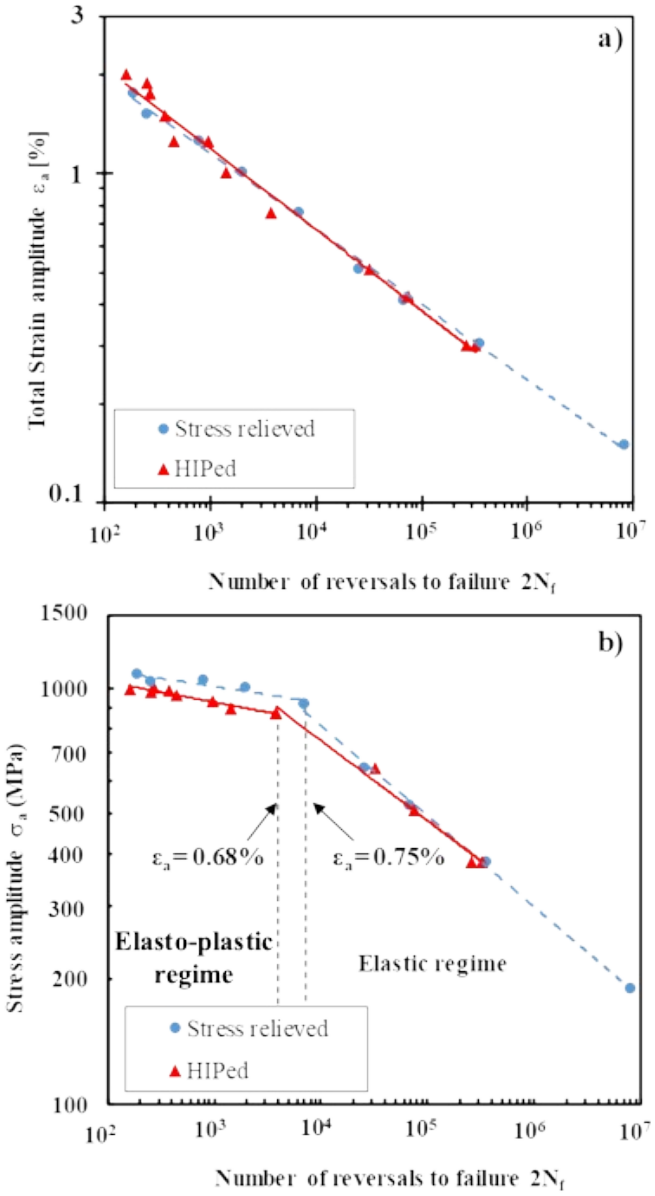

Figure 10. Fatigue performance. a) ε-N curves and b) S-N curves.

3.4.6. Strain energy vs fatigue life

The total strain energy density range was calculated as the sum of the plastic and the positive elastic strain energy density ranges of the mid-life hysteresis loops. It can be written by Eq. 6 [31,38].

$$\Delta W_T = kp(2Nf)^{ap} + \Delta W^{e+ii} \quad (6)$$

where *kp* and *αp* are material constants, and $\Delta W^{e+¿¿}$is the tensile elastic energy range at the material fatigue limit estimated here at $2N_f = 10^7$. Fig. 11a) and 11b) present the total strain energy density range of the mid-life hysteresis loops against the number of reversals to failure, for the stress relieved treatment and HIP treatment, respectively. Overall, the fitted Eq. 6 agrees well with the experimental results and can be used either in low or high cycle fatigue regimes. Table 3 summarizes the energy-based parameters for both stress relieved and HIPed samples.

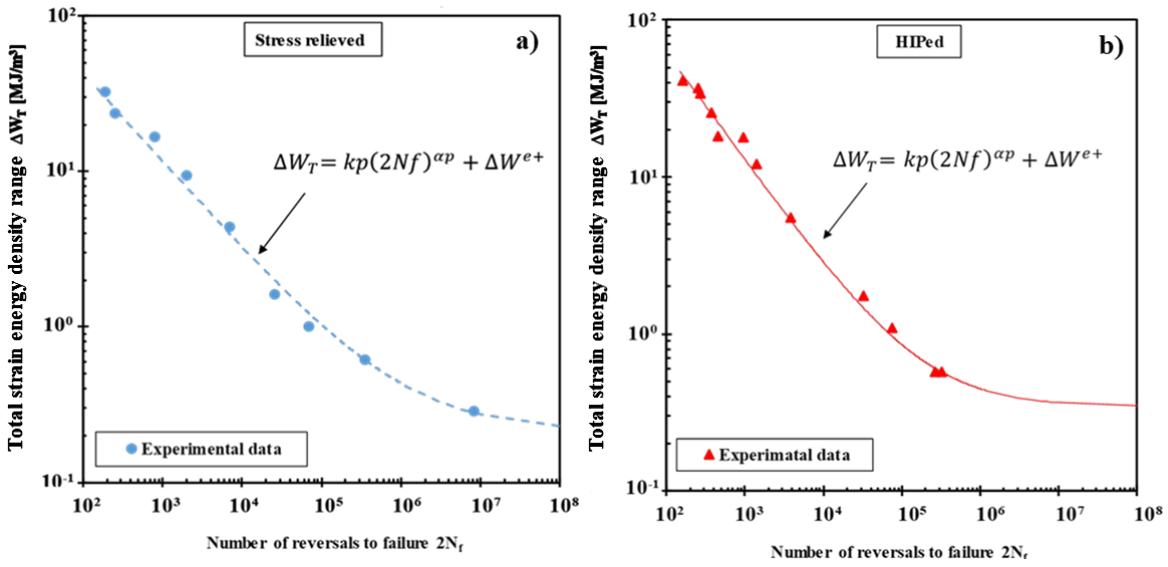

Figure 11. Total strain energy density range of the mid-life hysteresis loops vs number of reversals to failure: a) Stress relieved specimens; b) HIPed specimens.

3.5. Fatigue life predictions

Fig. 12 compares the S-N curves obtained for smooth and notched samples subjected to the stress relieved treatment. It is possible to conclude that the un-notched samples presented higher fatigue strength than the notched sample due to the presence of the notch that generates stress concentration. Once the tests were performed in deformation control and all the tests were performed in the predominantly elastic regime, the stress values were obtained by Hooke's law. The maximum local stresses plotted in Fig. 12 for the notched samples were calculated using Eq. 7 (taking into account that R=-1,$\sigma_{max} = \sigma_a$).

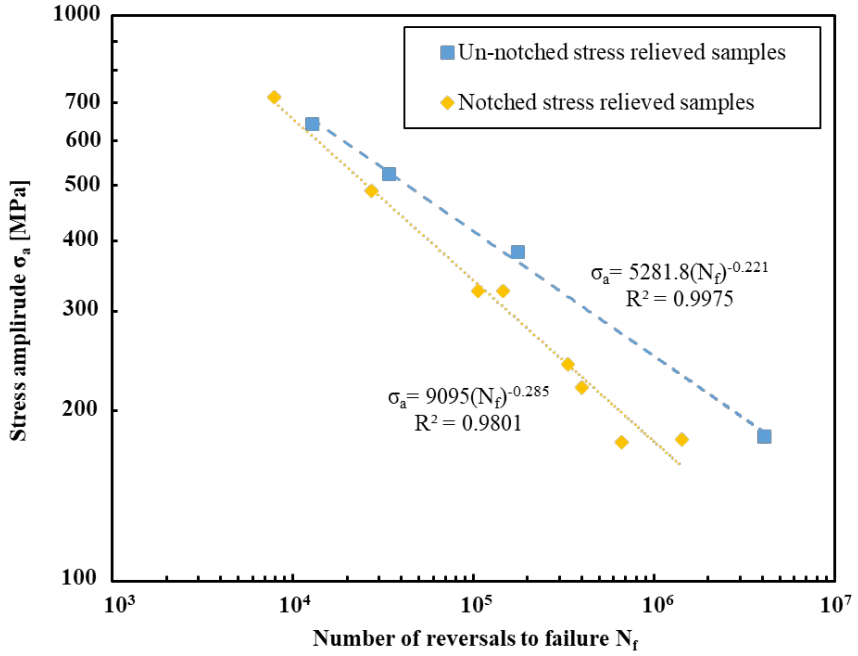

Figure 12. S-N curves for un-notched and notched stress relieved samples. R=-1.

Fatigue life predictions for the stress relieved notched specimens were performed using two different models: the SWT[39] (Smith-Watson-Topper) model and a model based on the total strain energy density (Eq. 6). Both approaches need to know the value of the static stress concentration factor. The static concentration factor, k_t, can be estimated by Eq. 7, where, σ_{max}, is the maximum stress at the notch root and σ_n the nominal stress.

$$k_t = \frac{\sigma_{max}}{\sigma_n} \tag{7}$$

The maximum stress, σ_{max}, was obtained by the finite element method (FEM) using the CAD software Autosesk Inventor®, assuming an isotropic linear elastic material. Through this software it was possible to create a precise model of the geometry of the notched specimens. The nominal stress, σ_n, was calculated by dividing the maximum applied load (10 kN) by the cross-section area of the notch, being estimated that $\sigma_{máx}$ =1326 MPa by FEM. Then, applying Eq. 7 a value of k_t=1.73 was obtained.

The fatigue stress concentration factor, k_f, was obtained by Eq. 8, where: σ_{fu} is the fatigue strength for smooth specimens and σ_{fe} the fatigue strength for notched specimens. These two parameters were calculated using the S-N relationships presented in Fig. 12 assuming $N_f = 10^7$. The estimated value of k_f was 1.63.

$$k_f = \frac{\sigma_{fu}}{\sigma_{fe}} \quad (8)$$

Using the values of the static and fatigue stress concentration factors it is possible to calculate the notch sensibility, q, using Eq. 9[40], being equal to 0.86 at the fatigue life of $N_f=10^7$.

$$q = \frac{k_f - 1}{k_t - 1} \quad (9)$$

This notch sensibility value of 0.86, being close to unity, indicates that this titanium alloy produced by SLM have a high sensibility to the presence of geometric discontinuities such as notches or surface defects resulting from the manufacturing process. Defining the fatigue strength as the stress amplitude for a fatigue life of $N_f= 10^7$a value of σ_{fu}=150 MPa is obtained. This value suffered a drastic reduction when compared to the fatigue strength of the wrought material, wich is σ_{fu}=410 MPa[40], ($N_f=10^7$, light polished samples and R=-1) due to a poor surface finish, porosity and detrimental residual stresses as reported by Wycisk et al.[4], Edwards et al.[5], Leuders et al.[6] and Cao et al.[7].

All maximum stresses in Fig. 12 are within the predominantly elastic regime, whereby the parameters used from Table 3 were those corresponding to $\varepsilon_a < 0.75$ %. Using the equation proposed by Smith-Watson-Topper (SWT)[39] based on strain-life testing data and the Eq. 7, the fatigue life can be predicted for the notched specimens by Eq. 10.

¿ (10)

For the model based on total strain energy density (Eq. 6), the total energy density ΔW_T was calculated by Eq.11 once all tests were in the predominantly elastic regime,

$$\Delta W_T = \frac{\Delta \sigma_{loc} \Delta \varepsilon_{loc}}{2} \quad (11)$$

where$\Delta \sigma_{loc}$is the maximum local stress ranges and $\Delta \varepsilon_{loc}$ is the maximum local strain ranges estimated through Hooke´s law. Predictions of the fatigue life were performed by Eq. 6 using the parameters presented in Table 3 for the stress relieved sample. Fig. 13a) and 13b) plot the fatigue life predictions versus experimental fatigue lifes for SWT and the energy model, respectively. There is a good correlation between predicted and experimental results once 100% of the points are within scatter bands with a factor of 2.

The SWT model gives non-conservative fatigue life predictions while the model based on the total strain energy density showed to be conservative.

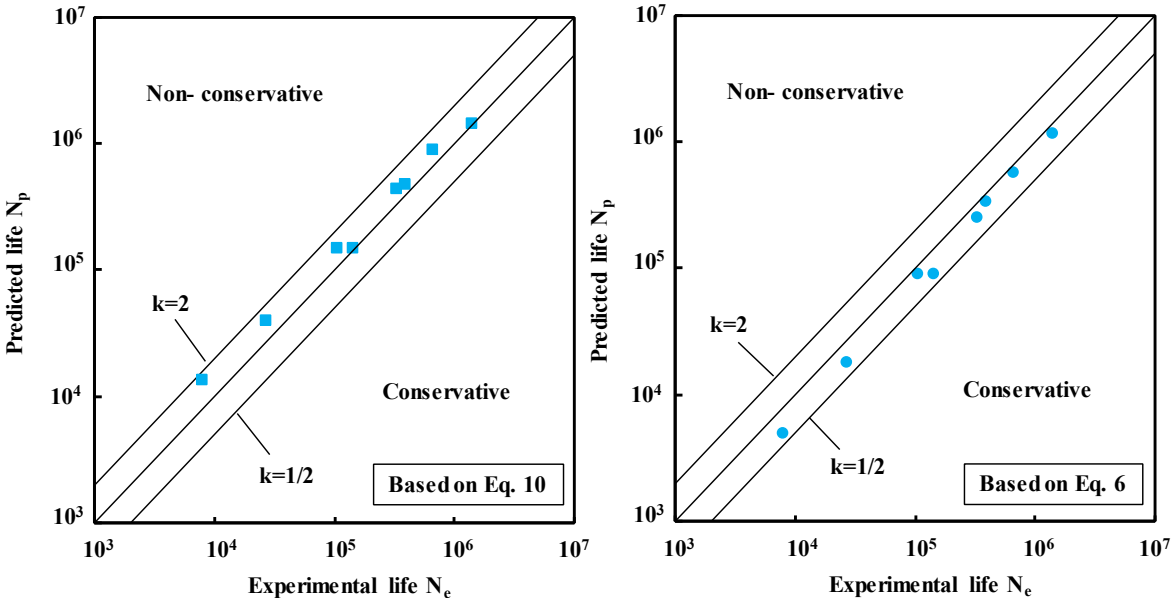

Figure 13. Fatigue life predictions versus experimental fatigue lifes. a) SWT model b) total strain energy density based model.

4. CONCLUSIONS

In this work, fatigue tests were performed (R_ε=-1) in samples produced by SLM in Ti6Al4V alloy in order to understand the influence of two heat treatments (stress relief and the HIP treatment) on the fatigue behaviour. Fatigue life predictions were also performed using two different prediction models for notched specimens. From this study the main conclusions drawn are the following:

- The application of HIP treatment caused a microstructural transformation leading to a loss of hardness and consequently a decrease of the monotonic mechanical properties;
- The stress relieved sample showed a cyclic softening while the HIPed sample did not alter its behaviour under cyclic deformation. In both cases a non-Masing behaviour was obtained.
- The elastic strain amplitude vs fatigue life curve presented a bilinear behaviour, explained by the Young´s modulus decreasing during the cyclic elasto-plastic tests as a consequence of the formation of a sub-grained microstructure;
- The HIP treatment reduces the fatigue strength in comparison with the stress relief treatment;

- Two fatigue life prediction models were successfully applied in notched stress relieved samples using the fatigue properties obtained in this work. The SWT model tended to be non-conservative while the model based on the total strain energy density showed to be conservative.

ACKNOWLEDGMENTS

The authors would like to acknowledge the sponsoring under the project no. 028789, financed by the European Regional Development Fund (FEDER), through the Portugal-2020 program (PT2020), under the Regional Operational Program of the Center (CENTRO-01-0145-FEDER-028789), and the project POCI-01-0247-FEDER-042536, financed by European Funds, through program COMPETE2020, under the Eureka smart label S0129-AddDies. Finally, FEDER funds through the program COMPETE– Programa Operacional Factores de Competitividade – and by national funds through FCT– Fundação para a Ciência e a Tecnologia , under the project UIDB/00285/2020.

CONFLICT OF INTEREST

The authors declare that they have no known competing financial interests or personal relationships that could have appeared to influence the work reported in this paper.

REFERENCES

[1] Gu, D.D.; Meiners,W.;Wissenbach, K.; Poprawe, R. Laser additive manufacturing of metallic components: Materials, processes and mechanisms. Int. Mater. Rev. 2013, 57, 133–164.

[2] Boyer, R.R. An Overview on the Use of Titanium in the Aerospace Industry. Mater. Sci. Eng. A 1996, 213: 103–114.

[3] Niinomi, M. Mechanical biocompatibilities of titanium alloys for biomedical applications. J. Mech. Behav.Biomed. Mater. 2008, 1, 30–42.

[4] Wycisk E., Solbach A., Siddique S., Herzog D., Walther F., Emmelmann C. (2014). Effects of defects in laser additive manufactured Ti-6Al-4V on fatigue properties, Phys Procedia 56, 371–378.

[5] Edwards P., Ramulu M. Fatigue performance evaluation of selective laser melted Ti–6Al–4V, Mater Sci Eng, A (2014) 598, 327–337.

[6] Leuders S., Thöne M., Riemer A., Niendorf T., Tröster T., Richard H.A., Maier H.J.. On the mechanical behaviour of titanium alloy Ti6Al4V manufactured by selective laser melting: Fatigue resistance and crack growth performance," Int. J. Fatigue 2013 48, 300–307.

[7] Cao F, Zhang T, Ryder MA, Lados DA. A review of the fatigue properties of additively manufactured Ti–6Al–4V. 2018, JOM 70 (3):349–357.

[8] Xuan, Y. and Nastac, L. TMS 2017 146th Annual Meeting & Exhibition Supplemental Proceedings (2017). Springer International Publishing. doi: 10.1007/978-3-319-51493-2.

[9] Zhang H, Dengke D., Haopu, S. An C., Experimental study of effect of post processing on fracture toughness and fatigue crack growth performance of selective laser melting Ti-6Al-4V, Chinese Journal of Aeronautics. Chinese Society of Aeronautics and Astronautics. doi: 10.1016/j.cja.2018.12.007.

[10] Atkinson, H. V. and Davies, S. Fundamental aspects of hot isostatic pressing: An overview, Metallurgical and Materials Transactions A (2000): Physical Metallurgy and Materials Science, 31(12), pp. 2981–3000. doi: 10.1007/s11661-000-0078-2.

[11] J. Eridon. Hot isostatic pressing of castings, Metals Handbook, Ninth Edition, Volume 15 Casting: 538-541 (1988).

[12] Victor Chastand, Philippe Quaegebeur, Wilson Maia, Eric Charkaluk, Comparative study of fatigue properties of Ti-6Al-4V specimens built by electron beam melting (EBM) and selective laser melting (SLM), Materials Characterization. Elsevier, 143 (2017), 76–81. doi: 10.1016/j.matchar.2018.03.028.

[13] Hanchen Yu, Fangzhi Li, Zemin Wang, Xiaoyan Zeng. Fatigue performances of selective laser melted Ti-6Al-4V alloy: Influence of surface finishing, hot isostatic pressing and heat treatments, International Journal of Fatigue, 120 (2018), pp. 175–183. doi: 10.1016/j.ijfatigue.2018.11.019.

[14] Wang, R. F., Li, Y. T. and An, H. P. (2012) 'Low Cycle Fatigue Behaviors of TI-6AL-4V Alloy Controlled by Strain and Stress', Key Engineering Materials, 525–526, pp. 441–444. doi: 10.4028/www.scientific.net/kem.525-526.441.

[15] Patricio E.Carrion, Nima Shamsaei, Steven R. Daniewicz, Robert D.Moserc 'Fatigue behavior of Ti-6Al-4V ELI including mean stress effects', International Journal of Fatigue 2017. Elsevier Ltd, 99, pp. 87–100. doi: 10.1016/j.ijfatigue.2017.02.013.

[16] Peng Zhang, Allen Naihui He, Fei Liu, Kaifei Zhang, Junjie Jiang, David Zhengwen Zhang. Evaluation of Low Cycle Fatigue Performance of Selective Laser Melted Titanium Alloy Ti–6Al–4, Metals 2019, 9 (10), 1041.

[17] Xu, H., Ye, D. and Mei, L. 'A study of the back stress and the friction stress behaviors of Ti-6Al-4V alloy during low cycle fatigue at room temperature', Materials Science and Engineering A (2017). Elsevier B.V., 700(November), pp. 530–539. doi: 10.1016/j.msea.2017.06.051.

[18] Duyi Ye, Dehai Ping Zhenlin Wang, Haohao Xu, Xiaoyu Mei, Changwei Xu, Xiaolin Chen. Low cycle fatigue behavior of nickel-based superalloy GH4145/SQ at elevated temperature, Materials Science and Engineering A, 373(1–2), pp. 54–64. doi: 10.1016/j.msea.2004.01.045.

[19] K.Gopinatha, A.K.Gogia, S.V.Kamat, R. Balamuralikrishnan, U. Ramamurty 'Low cycle fatigue behaviour of a low interstitial Ni-base superalloy', Acta Materialia. Acta Materialia Inc. (2009), 57(12), pp. 3450–3459. doi: 10.1016/j.actamat.2009.03.046.

[20] R.Branco, J.D.Costa, L.P.Borrego, S.C.Wu, X.Y.Long, F.C.Zhang. Effect of strain ratio on cyclic deformation behaviour of 7050-T6 aluminium alloy, International Journal of Fatigue, 129 (August), p. 105234. doi: 10.1016/j.ijfatigue.2019.105234.

[21] N.E. Prasad, G. Malakondaiah, P.R. Rao, Low cycle fatigue behaviour of an un-deraged Al-Li-Cu-Mg alloy, Trans.-Indian Inst. Met. 57 (2004) 181–194.

[22] Singh, N., Gouthama, Singh, V. Low cycle fatigue behavior of Ti alloy IMI 834 at room temperature, Materials Science and Engineering A . (2002), 325 (1–2), pp. 324–332. doi: 10.1016/S0921-5093(01)01468-X.

[23] ASTM E606 / E606M - 19 Standard Test Method for Strain-Controlled Fatigue Testing.

[24] ASTM E3 - 11(2017) Standard Guide for Preparation of Metallographic Specimens Active Standard ASTM E3 | Developed by Subcommittee: E04.01 Book of Standards Volume: 03.01.

[25] ASTM E407 - 07(2015). Standard Practice for Microetching Metals and Alloys

[26] ASTM Standard E384 (2011) Standard test method for Knoop and Vickers hardness of materials. ASTM International, West Conshohocken. https://doi.org/10.1520/E0384-11E01, www.astm.org

[27] ASTM B528 –16 Standard Test Method for Transverse Rupture Strength of Powder Metallurgy (PM) Specimens.

[28] Greitemeier D, Palm D, Syassen F, Melz T (2017) Fatigue performance of additive manufactured Ti-6Al-4V using electron and laser beam melting. Int J Fatigue 94:211–217.

[29] Molaei, R., Fatemi, A. and Phan, N. (2018) 'Significance of hot isostatic pressing (HIP) on multiaxial deformation and fatigue behaviors of additive manufactured Ti-6Al-4V including build orientation and surface roughness effects', International Journal of Fatigue. Elsevier, 117(April), pp. 352–370. doi: 10.1016/j.ijfatigue.2018.07.035.

[30] Osgood, W.R.; Ramberg, W. Description of Stress-Strain Curves by Three Parameters; National Advisory Committee for Aeronautics: Washington, DC, USA, 1943; pp. 1–13.

[31] Ricardo Branco, José D. M. Costa, Filippo Berto, Seyed Mohammad Javad Razavi, José A. Martins Ferreira, Carlos Capela, Luís Santos and Fernando Antunes (2018) 'Low-Cycle Fatigue Behaviour of AISI 18Ni300 Maraging Steel Produced by Selective Laser Melting', Metals, 8(1) 32. doi: 10.3390/met8010032.

[32] Basquin, O.H. The Exponential Law of Endurance Testing (1910). Am. Soc. Test. Mater., 19, 625–630.

[33] M. Yang, Y. Akiyama, T. Sasaki (2004) "Evaluation of change in material properties due to plastic deformation", Journal of Materials Processing Technology 151 (2004) 232–236.

[34] Jyoti S. Jha, Satyabrat Dhala, Suraj P. Toppo, Rajkumar Singh, Asim Tewari, Sushil K. Mishra, Bhagyaraj Jayabalan (2019) ”Effect of strain amplitude on low cycle fatigue and microstructure evolutionin Ti-6Al-4V: A TKD and TEM characterization”, Materials Characterization 155, 109829.

[35] Manson, S.S. “Behavior of Materials Under Conditions of Thermal Stress” (1953), Technical Report TN 2933; NACA: Boston, MA, USA.

[36] Conffin, L.F., Jr. “A Study of the Eects of Cyclic Thermal Stresses on a Ductile” (1954), Metal. Trans. Am. Soc. Mech. Eng.76, 931–950.

[37] Morrow J. D. “Cyclic plastic strain energy and fatigue of metals”. Int. Friction, Damping and Cyclic Plasticity (1965), ASTM, STP 378. American Society for Testing and Materials, Philadelphia, pgs. 45-87.

[38] Branco, R, Costa, J.D, Berto, F, Antunes, F.V. “Fatigue life assessment of notched round bars under multiaxial loading based on the total strain energy density approach” (2017), Theor. Appl. Fract. Mech. 97, 340-348.

[39] Smith KN, Watson P, Topper TH “A stress–strain function for the fatigue of metals” (1970). J Mater 5:767–778.

[40] Marc Long, H.J.Rack, “Titanium Alloys in Total Joint Replacement- A Materials Science Perspective” (1998), Biomaterials 19 1621-1639.